International Journal of Research in Advent Technology, Vol.2, No.5, May 2014
E-ISSN: 2321-9637

Comparative Study and Design of Optical XNOR and NAND Logic Gates

Manisha[1], Biram Chand Khorwal[2], Gaurav Saini[3]
Department of Electronics & Communication[1, 2, 3], AIACTR, GGSIPU,New Delhi[1, 2, 3,]
Email: manishabainsla89@gmail.com,khorwal007@hotmail.com,saini.grv15@gmail.com[1]

Abstract -We present two design method and potential application for optical XNOR and NAND gates. In first design technique Light propagation in a 2-D array of coupled optical cavities with Kerr nonlinearity driven by a plane holding beam is numerically studied. 2-D discrete cavity solitons are simulated. Soliton–soliton and soliton–GB interactions are considered, and optical XNOR, and NAND gates are proposed. In second design technique the binary- phase-shift-keyed signal processing devices are composed of multi-mode interference waveguides and convert the phase information of the input signal to amplitude at the output. We apply the finite element method for numerical simulations, and the evaluated least ON to OFF logic-level contrast ratios for the XNOR, and NAND, logic gates are , 21.5 dB and 22.3 dB, , respectively.

Index Terms- Binary-phase-shift-keyed modulation format, multi-mode-interference, optical logic gate

1. INTRODUCTION

For many years, optics scientists have been looking for all-optical signal processing materials that enable one light beam to be controlled by another. Studies on light localization in discrete optical systems have taken much interest. The peculiarities of discrete diffraction allow for the formation of new types of spatially localized solutions, so-called discrete solitons[1-3]. An array of coupled-waveguide resonators is constructed through addition of mirrors to the input and output facets of the waveguide array, which is excited by an external driving field [4]. Multiple reflections of light on the mirrors increase in light interaction with the nonlinear material inside the cavity causes to form discrete cavity solitons (DCSs) at substantially less powers in comparison with conventional spatial solitons in single pass configuration. Simultaneous excitation of bright and dark DCSs in the same array of coupled waveguides is one of unique features of these systems. The first observation of a 2-D discrete soliton was achieved in optically induced waveguide arrays in photorefractive materials [5]. A number of experimental and theoretical studies on all-optical logic gates using optical Kerr effect as a switching mechanism have been reported [6]–[9]. Optical packet switching systems have some advantages, such as high throughputs, low power consumption, and high band efficiency, compared to conventional electrical routers. However, different modulation formats will be selectively used according to different network scales and applications in future networks [10], [11].
Differential-phase-shift-keyed (DPSK) receivers have been studied for many years [12], and the use of the delay-interferometer with direct detection has been extensively studied [13], [14]. Compared to the OOK formats, the DPSK formats have the advantage of a 3-dB reduction in the required optical signal-to-noise ratio (OSNR) [15], [16]. In this paper, work is to introduce 2-D DCSs in Kerr media. This feature of solitons is different compared with its one-dimension counterpart. We will show that appropriate Gaussian beam (GB) can be used as a control beam to switch on/off DCSs and to route them, providing an effective tool to use in all-optical logic gates. After that the possibility of optical controlling of solitons and its mutual interactions is investigated by demonstrating, XNOR, and NAND logic gates and also we propose optical XNOR and NAND logic gates with coherent detection based on multi-mode interference (MMI) waveguides for BPSK signals. The optical logic gates include functions as phase-to-amplitude converters and operate as logic gates, as shown in Fig. 1. In the optical logic gates, the logical value of the input is determined by the phase information, whereas the logical value of the output is determined by the amplitude. Moreover, we adopt silicon-based multi-mode interference (MMI) waveguides for the base structure of the logic gates because MMI-based devices have several advantages, including their simple configuration, large bandwidth, and compact size [15]–[16]. We employ the finite element method (FEM) [17] for numerical simulations and calculate the spectrum of the ON to OFF logic-level contrast ratio. Consequently, the least ON to OFF logic-level contrast ratios for the XNOR and NAND logic gates were 21.5 dB and 22.3 dB, respectively.

2. MODEL

In first technique consider a 2-D array of weakly coupled parallel waveguides with Kerr nonlinearity (see Fig. 1).

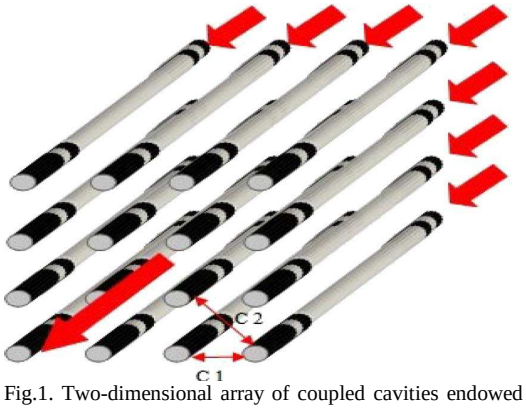

Fig.1. Two-dimensional array of coupled cavities endowed with a Kerr nonlinearity.

The main assumption is that the evolution of the slowly varying envelopes of the individual guided modes can be described by a discrete equation, taking into account the nearest neighbor interaction of the weakly overlapping guided modes. We assume that the cavities are in resonant with the operating frequency and a mean-field approach can be applied. General discrete model for the normalized amplitude $u_{n,m}$ excited by external driving field E0 is (Fig. 1):

$$i\frac{\partial u_{n,m}}{\partial t}+C_1(u_{n+1,m}+u_{n-1,m}+u_{n,m+1}+u_{n,m-1}-4u_{n,m})$$
$$+C_2(u_{n+1,m+1}+u_{n+1,m-1}+u_{n-1,m-1}-4u_{n,m})$$
$$+(\Delta+i)u_{n,m}+\gamma\left|u_{n,m}\right|^2 u_{n,m}=E_0 e^{i(q_1 n+q_2 m)} \quad (1)$$

All quantities are dimensionless, the evolution time, t , is scaled to photon lifetime and the field amplitudes to effective nonlinear coefficient [8], [26]. $u_{n,m}$ is the field amplitude in site (n,m), Δ stands for detuning from the cavity resonance, and C1 and C2 are different neighbour coupling between non diagonal and diagonal cavities, respectively. The evanescent coupling coefficient decreases exponentially with increasing distance between adjacent waveguides. For simplicity, the ratio C1/C2 is kept constant to √2. The last term at left is self-focusing Kerr nonlinearity in waveguides for $\gamma=+1$ .q_1 and q_2 are terms for vertical and horizontal phase shifts between the fields in adjacent cavity inputs that depend on inclination of the holding beam with amplitude E_0.

2.1 DCS

The theory of DCSs is often based on the discrete NLS equation, and it is valid for weakly coupled waveguides. Here, bright DCSs that propagate along 2-D arrays of cavities endowed with a Kerr nonlinearity are found numerically for a 1-D and a 2D lattice (see Fig. 2) when holding beam incident normally to the input facet (q1 = q2 = 0).

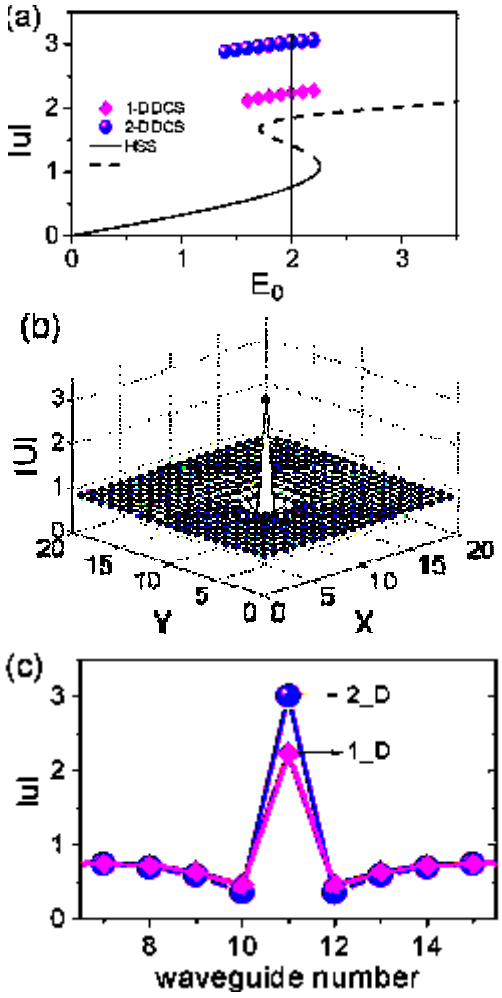

Fig. 2. (a) Families of bright DCSs are shown as maximum modulus of the field amplitude for 1-D (diamond) and for 2-D (circle) with PW solution (solid line: stable and dashed: unstable) versus holding beam amplitude, E0. (b) Amplitude distribution of 2-D stable DCS. (c) Profiles of DCSs in 1-D (diamond) and 2-D (circle) waveguide array. (Parameters: E0 =2, C1 = 0.8, Δeff =-3.)

Newton–Raphson and fourth-order Runge–Kutta methods are used to estimate steady solution of (1) and to investigate time evolution of outgoing beam, respectively. Fig.3 shows that stable DCS in 2-D not only has larger peak intensity but also exists in a wider range of holding beam with respect to its 1-D counterpart.

2.2 Controlling of DCSs

The interaction between spatial solitons has attracted much attention because they resemble real particles in the interaction properties. In order to optimize the routing/steering process, all-optical control of spatial solitons is highly desirable [13]. In this section, we demonstrate some all-optical controlling of DCS by applying appropriate Gaussian control beam to write, erase and to route.

2.2.1 Switching (Writing and Erasing)

In order to write and erase DCSs in a given site (n;m), we assume holding beam E as a superposition of

PW, E_0 and a GB, E_1 as:

$$E = E_0 + E_1 e^{-(n^2+m^2)/w^2} e^{i\phi} \qquad (2)$$

where w and ϕ specify width and phase of GB, respectively. Other parameters are fixed as previous section as E_0 = 2, C_1 = 0.8, C_2 = 0.57, and normal incident holding beam is considered, i.e., q1 = q2 = 0. The process of writing and erasing of DCS is almost the same, in which GB is injected during t_{inj} , (ϕ=0) for writing and out of phase (ϕ=π) for erasing. The switching process involves two stages: first, injecting of GB, and in the second stage, the system is left to relax to its final stable state.

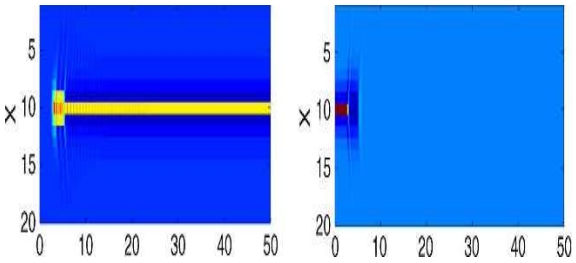

Fig. 3. Panel shows the space–time contour plot of the modulus amplitude of holding beam during writing (left) and erasing (right) processes.

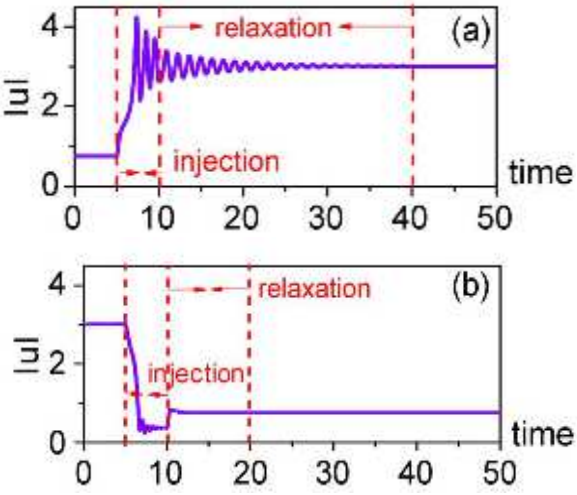

Fig. 4. Time evolutions of peak amplitude during writing and erasing processes in (a) and (b), respectively.

Intensity distributions in adjacent waveguides are shown in Fig. 3. Time evolution of the amplitude during writing and erasing processes and time are plotted in Fig. 4. Successful writing and erasing takes place when injection time of GB exceeds a lower threshold depending upon E_1 and w (see Fig. 5). For this purpose, we achieved minimum time of control beam for switching (writing and erasing) by increasing control beam amplitude as well as increasing its beam width.

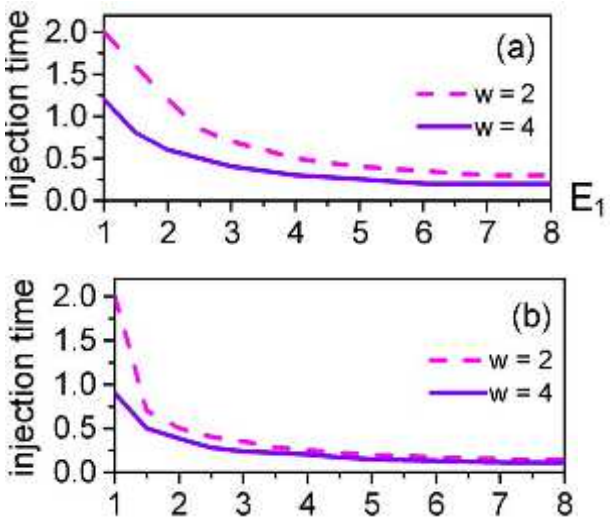

Fig. 5. Injection time versus amplitude of GB E1 for writing and erasing processes in (a) and (b),respectively, for two different beam widths.

2.2.2 All-Optical NOR, XNOR, and NAND Gates Based on DCS Interaction

One of the main characteristics of bistable systems is having two distinguished states for the same parameters, which can be considered as logic signal 0 or 1.

Consider two near waveguides named A and B are our input for logic signals. A stable bright soliton in A or B means our signal sets as 1; otherwise, it is 0. For these two near guides to be independent, their distance was chosen to be about 4 waveguides. The control beam that determines the type of gates is considered as a GB in the form of (5) injected at the waveguide C placed between guides A and B in a short time interval t_{inj} . The gate output is also taken from C after a short time. Interaction of control beam with optical fields in A and B depends on the beam's intensity. Different kinds of gates (XNOR, and NAND) are designed by well adjusting the intensity of control beam and keeping the injection time fixed at t_{inj} = 8, all of which are described in the following subsections in detail.

2.2.2(a) XNOR Gate

Fig. 6 illustrates an exclusive-NOR (XNOR) gate if the injected amplitude of control beam in C is E_1 = 9. Control beam can deflect the signal-carrying solitons A or B in each neighbor waveguides, whereas the out port is active only when both or none of A and B are launched.

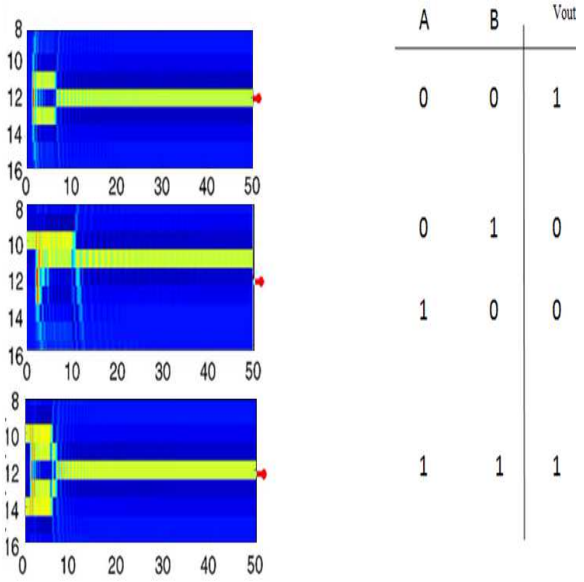

Fig. 6. XNOR gate with three soliton-forming beams. The control and two signal beams time evolutions. From top to bottom: both A and B are off (00) only A (B) on (10), (01), both A and B on (11). The arrow indicates the output channel. Control beam amplitude is E1 = 9, and injection time is tinj = 8. Other parameters are E0 = 2, C1 = 0.8, C2 ¼=0.57, Δeff =-3.

2.2.2(b) NAND Gate

Fig. 7 is an example of a NAND gate that shows the propagation of A, B, and C, whereas soliton C displays the signal output. As it is apparent from Fig. 7, the output is on when both of the signals are present or absent (with C injected byE_1=5).

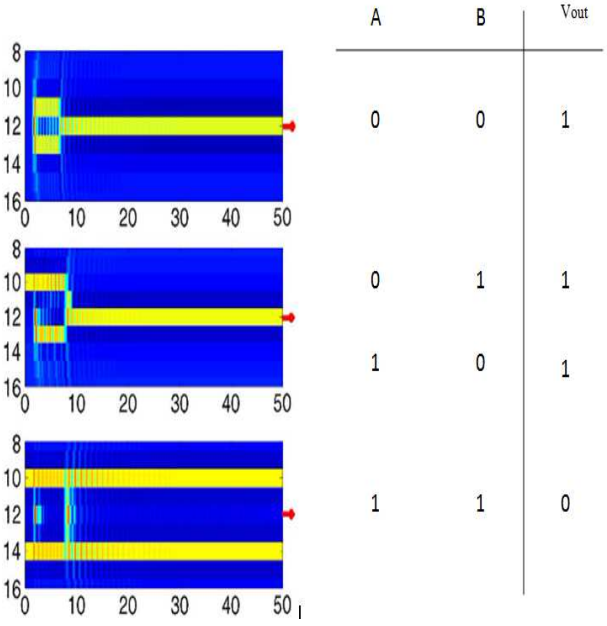

Fig. 7. NAND gate with three soliton-forming beams. The control and two signal beams time evolutions. From top to bottom: both A and B are off (00) only A (B) on (10), (01), both A and B on (11). The arrow indicates the output channel. Control beam amplitude is E1 = 5, and injection time is tinj = 8. Other parameters are E0 = 2, C1 = 0.8, C2 = 0.57, Δeff =-3.

3. BASIC MMI THEORY

MMI devices are based on the self-imaging property, in which the guided modes of a MMI region are excited and interfere constructively when a smaller input field of input waveguide is launched.

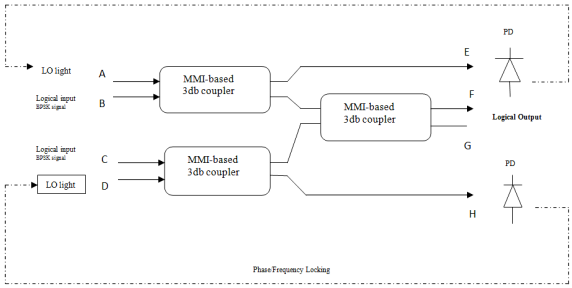

Fig.8.Schematic of the optical XNOR and NAND logic gates

Then, the excited fields in MMI region transmute periodically along the propagation direction. Here, the beat length in the MMI region is given by

$$L_\pi = \frac{\pi}{\beta_0 - \beta_1} = \frac{\lambda}{2(n_{eff\,0} - n_{eff\,1})} \qquad (3)$$

where β_0 and $\beta_1$indicate the propagation constant of the fundamental mode and first-order mode, respectively, n_{eff0} and n_{eff1} represent the effective refractive indexes of the fundamental mode and first-order mode, respectively, and λ is the wavelength. From the MMI theory [20], (1) is rewritten as follows:

$$L_\pi \cong \frac{4 n_c W^2{}_{eff}}{3\lambda} \qquad (4)$$

Where n_c and W_{eff} are the refractive index and effective width of the MMI region, respectively. In the two-input waveguide case, there are two self-imaging mechanisms. One is the general interference (GI). In this case, the distance of first -fold images is defined as

$$L = \frac{3L_\pi}{N} \qquad (5)$$

Where N>=1 is integer. The other mechanism is the restricted interference (RI). In this case, L is defined as

$$L = \frac{L_\pi}{N} \qquad (6)$$

From (5) and (6), it can be seen that the coupling length of the RI mechanism is three times shorter than that of the GI mechanism.

3.1. DESIGN PRINCIPLE OF MMI

Here, we describe how to design W_{MMI} and L_{MMI} of the MMI-based 3-dB coupler as shown in Fig. 9.

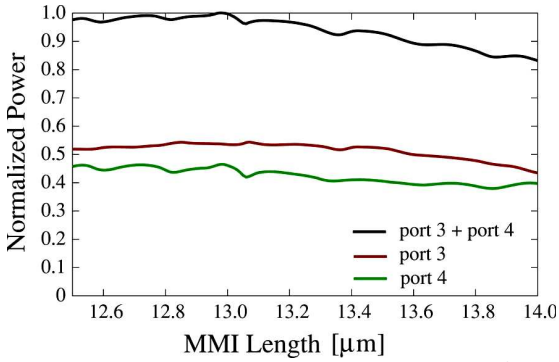

Fig. 9. Normalized power variation changing the L_{MMI} from 12.5 μm to14.0 μm.

From (4), it is obvious that as the width of MMI region is wider, the length of the MMI region becomes longer.

Accordingly, we select W_{MMI} =3.0μm so that the total size of the device is as small as possible. When we set W_{MMI} =3.0μm, and assuming, from (4) and (6), we can see that becomes 13.5μm at λ=1.55μm (first 2-fold images). Next, we calculate the distance of first 2-fold images from (3).

By using the mode-analysis-FEM solver, $n_{eff\ 0}$ =3.49 and $n_{eff\ 1}$ =3.46 for the TM mode are obtained. As a result, L becomes 13.7 μm at λ=1.55μm from (6). This result is in excellent agreement with that from (4). Fig. 9 shows that the normalized power variation changes the form 12.5 μm to 14.0 μm for the TM mode at λ=1.55μm launched into port 1. We ultimately choose L_{MMI} =13.0μm to achieve the highest transmission.

3.2 MMI Based 3-dB Coupler

To explain the operation principle of the MMI-based 3-dB coupler, at first, we consider that a beam is inputted into port 1. Because the 3-dB coupler is treated, the power is equally divided between port 3 and port 4. Then, the phase difference between port 3 and port 4 is consistently "π/2". Under this condition, we assume that the phase on port 3 and port 4 are, respectively, π/2 and 0, as shown in Fig. 10(a) (State 1). If a beam having the same phase for State 1 is inputted into port 2, the phase in port 3 and port 4 become 0 and π/2 , respectively, as shown in Fig. 10(b) (State 2). Then, we consider the case in which beams are inputted with the same phase into both port 1 and port 2. Now, because our proposed structure is a linear device, the structure satisfies the principle of superposition. Thus, it is able to add the complex amplitude of State 1 and State 2, and the lights on port 3 and port 4 have the same phase and amplitude, as shown in Fig. 10(c). Next, we consider the condition that there exists a certain phase difference between port 1 and port 2. If the phase difference is +π/2(the phase at port 2 is faster than that of port 1), the phase lead of outputted lights is π/2 compared to the output phase relation of State 1. In this case, the lights on port 4 are negated due to the opposite phase, and

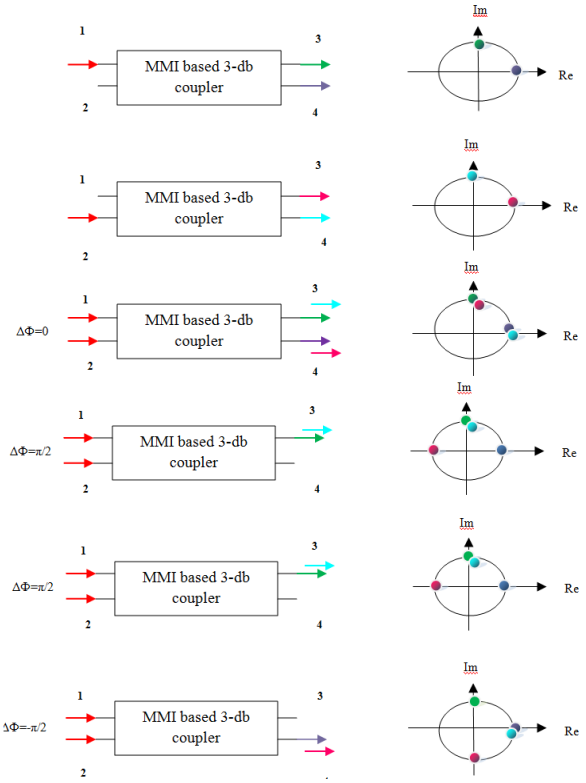

Fig.10. (a, b, c, d, e, f) the operation principle of the MMI-based 3-dB coupler.Δϕ is the phase difference between port 1 and port 2. The color of the arrow corresponds to the dot on the complex plane.

consequently, the light is outputted from only port 3, as shown in Fig. 10(d). However, if the phase difference is –π/2 (the phase at port 2 is slower than that of port 1), the phase lag of outputted lights is π/2 compared to the output phase relation of State 1. Then, the light on port 3 is negated due to the opposite phase, and consequently, the light is outputted from only port 4, as shown in Fig. 10(e). We apply these physical phenomena to the basic operating principle of the logic gates. Thus, the MMI-based 3-dB coupler fulfils the role of converter that converts the phase information of the input signal to amplitude at the output.

In practice, there is a phase error between the BPSK signal and the LO light. Therefore, the conversion efficiency when there is the phase error becomes an important indicator for practical implementation. The conversion efficiency is defined as

$$\eta = \frac{P_{port3}}{P_{\max}} * 100 \qquad (5)$$

where, P_{max} and P_{port3} are, respectively, the maximum output power and the power of port 3. Moreover, we show the insertion loss of the MMI-based 3-dB coupler.

The insertion loss IL is defined as

$$IL = 10\log_{10}\frac{P_{port3} + P_{port4}}{P_{port1}} \qquad (6)$$

where P_{port1} and P_{port3} + P_{port4} are, respectively, the normalized input power and the total output power.

3.3 NUMERICAL RESULT AND DISCUSSION

A. XNOR Logic Gate

To realize an XNOR logic gate, we assume the ideal conditions that the phases of the LO light on ports A and D are π/2 and 0, respectively. Moreover, we suppose the same wavelength and polarization between the input-signal light and the LO light. In the BPSK format, the 0-phase corresponds to logic 0, whereas the π -phase corresponds to logic 1. Here, we assume that a π/2 phase sifter is inserted in front of port C to realize an XNOR logic gate. In this way, on port C, π/2 -phase corresponds to logic 0, whereas –π/2 phase corresponds to logic 1. If these requirements have been satisfied, the XNOR logic gate operates as follows.

1) When an input-beam on port B has a phase ϕ=0 (corresponding to logic 0) and an input-beam on port C has Φ=π/2 (corresponding to logic 0), logic 1 is obtained from port F.

2) When an input-beam on port B has ϕ=0 (corresponding to logic 0) and an input-beam on port C has Φ=-π/2(corresponding to logic 1), logic 0 is obtained from port F.

3) When an input-beam on port B has a phase ϕ=π (corresponding to logic 1) and an input-beam on port C has Φ=π/2(corresponding to logic 0), logic 0 is obtained from port F.

4) When an input-beam on port B has ϕ=π (corresponding to logic 1) and an input-beam on port C has ϕ=-π/2 (corresponding to logic 1), logic 1 is obtained from port F.

These operations are summarized in Table I.

FUNCTIONS OF THE XNOR LOGIC GATE

Logical input				Logical output
B		C		F
Logic	Φ	Logic	Φ	Logic
0	0	0	π/2	1
0	0	1	-π/2	0
1	π	0	π/2	0
1	π	1	-π/2	1

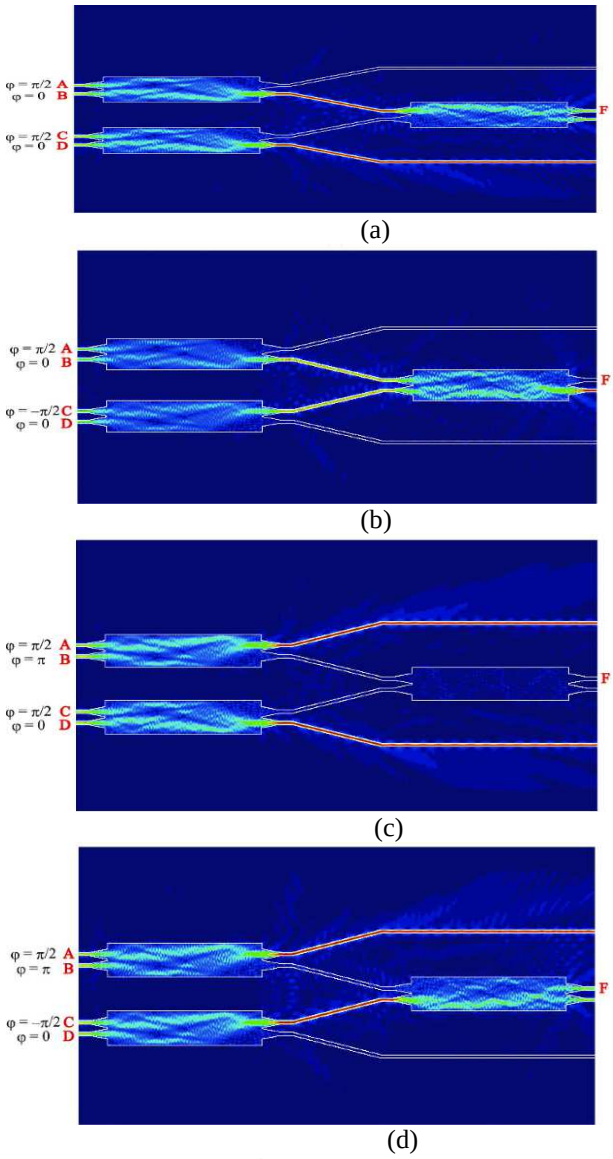

Fig. 11. Field distributions of the XNOR logic gate at an operating wavelength of λ=1.55μm. (a)-(d) correspond to explanations of the XNOR operation (1)–(4), respectively.

To gain more insight into the physics of the XNOR logic gate, the field distributions at λ=1.55μm are illustrated in Fig. 10, from which it is recognized that the structure functions as an XNOR gate. For the XNOR logic gate, the smallest ON to OFF logic-level contrast ratio is 21.5 dB.

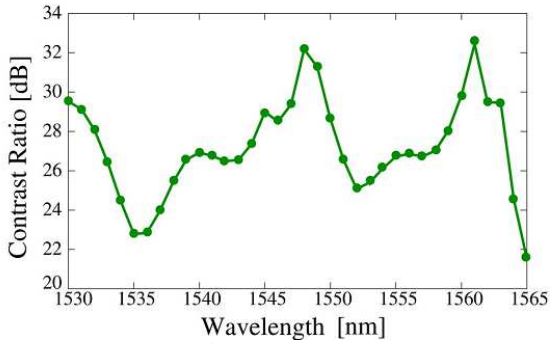

Fig. 12. The spectrum of the ON to OFF logic-level contrast ratio for the XNOR logic gate

B. NAND Logic Gate

To realize the NAND logic gate, we assume the ideal conditions that the phase of the LO light on ports A and D is π/2 when the phase of the BPSK signal is 0 or π. Moreover, we assume the same wavelength and polarization between the input-signal light and the LO light. If these requirements have been satisfied,
the NAND logic gate operates as follows:
1) When an input-beam on port B has ϕ=0(corresponding to logic 0) and an input-beam on port C has ϕ=0(corresponding to logic 0), logic 1 is obtained from port F.
2) When an input-beam on port B has ϕ=0(corresponding to logic 0) and an input-beam on port C has ϕ=π (corresponding to logic 1), logic 1 is obtained from port F.
3) When an input-beam on port B has a phase ϕ=π (corresponding to logic 1) and an input-beam on port C has ϕ=0(corresponding to logic 0), logic 1 is obtained from port F.
4) When an input-beam on port B has ϕ=π (corresponding to logic 1) and an input-beam on port C has ϕ=π (corresponding to logic 1), logic 0 is obtained from port F.
These operations are summarized in Table II.

FUNCTIONS OF THE NAND LOGIC GATE

Logical input				Logical output
B		C		F
Logic	Φ	Logic	Φ	Logic
0	0	0	0	1
0	0	1	π	1
1	π	0	0	1
1	π	1	π	0

To gain more insight into the physics of the NAND logic gate, the field distributions at λ=1.55μm are illustrated in Fig. 13, from which it is recognized that

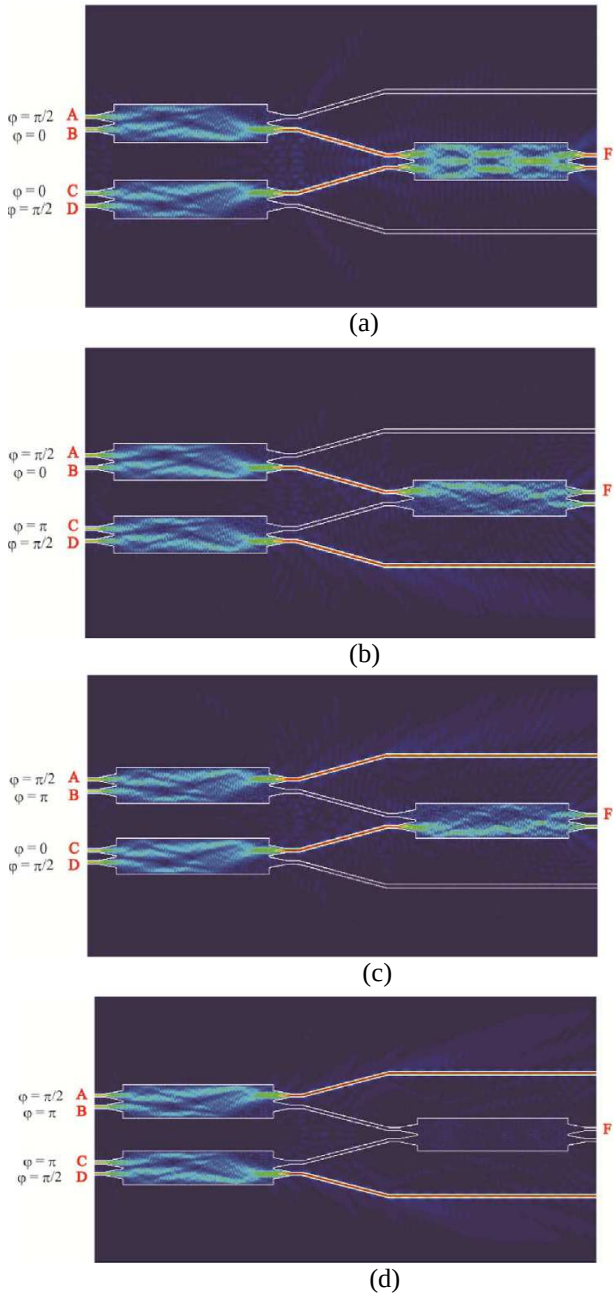

Fig. 13. Field distributions of the NAND logic gate at an operating wavelength of m. (a)–(d) correspond to explanations of the NAND operation (1)–(4), respectively

the structure functions as NAND gate. Fig. 12 shows the spectrum of the ON to OFF logic-level contrast ratio for the NAND logic gate. Here, we should add that there are three logic 1 states in the NAND operation, but we need to evaluate the worst state in which the least light intensity on port F is obtained. Therefore, we choose the NAND operation of (iii) as the logic 1 state in the calculation of contrast ratio. Then, the smallest ON to OFF logic-level contrast ratio is 22.3 dB in the whole C-band.

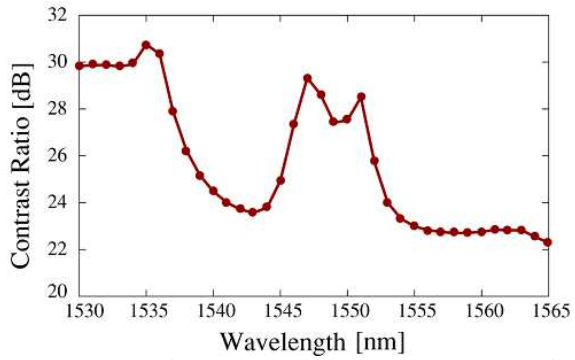

Fig. 12. Spectrum of the ON to OFF logic-level contrast ratio for the NAND
logic gate.

4. CONCLUSION

In this paper, in first technique we have investigated 2-D arrays of coupled optical fiber shape cavities. In second technique we have proposed optical XNOR and NAND logic gates based on MMI waveguides for BPSK modulation formats in packet switching systems.

In first technique successful switch (on/off) of solitons takes place if injection time of writing/erasing beam exceeds a minimum threshold, which is inversely proportional to the amplitude as well as width of the beam. The subsequent section involves the interaction of three propagating beams in 2-D adjacent waveguides. This property is used to demonstrate all-optical logic gates, namely XNOR, and NAND. This technology also could allow for several further all optical devices for communication and information processing.

While in second technique the device operations for the TM mode have been simulated and analyzed by FEM. Moreover, we have evaluated the device performance. The least ON to OFF logic-level contrast ratios for the XNOR and NAND were 21.5 dB and 22.3 dB, respectively. The proposed optical logic gates have great potential to simplify label processing systems for BPSK signals in future optical networks. Future attractive issues include experimentally proving the benefits of our approach in detail and constructing label recognition circuits by using our proposed optical logic gates.

REFERENCES

[1] F. Lederer, S. Darmanyan, and A. Kobyakov,Discrete Solitons in Spatial Solitons, S. Trillo and W. Torruellas, Eds. New York: Springer- Verlag, 2001.

[2] A. Fratalocchi, G. Assanto, and K. A. Brzdakiewicz, BDiscrete propagation and spatial solitons in nematic liquid crystals,[Opt. Lett., vol. 29, no. 13, pp. 1530–1532, Jul. 2004.

[3] A. Fratalocchi and G. Assanto, BDiscrete light localization in one-dimensional nonlinear lattices with arbitrary nonlocality,[Phys. Rev. E, Stat. Phys. Plasmas Fluids Relat. Interdiscip. Top., vol. 72, no. 6, p. 066608, Dec. 2005.

[4] U. Peschel, O. A. Egorov, and F. Lederer,BDiscrete cavity solitons,[Opt. Lett., vol. 29, no. 16, pp. 1909–1911, Aug. 2004.

[5] J. Fleischer, M. Segev, N. Efremidis, and D. Christodoulides, BObservation of two-dimensional discrete solitons in optically induced nonlinear photonic lattices,[Nature, vol. 422, no. 6928, pp. 147–150, 2003.

[6] T. Yabu, M. Geshiro, T. Kitamura, K. Nishida, and S. Sawa, BAll-optical logic gates containing a two-mode nonlinear waveguides,[IEEE J. Quantum Electron., vol. 38, no. 1, pp. 37–46, Jan. 2002.

[7] Y. D. Wu, BAll-optical logic gates by using multibranch waveguide structure with localized optical nonlinearity,[IEEE J. Sel. Topics Quantum Electron., vol. 11, no. 2, pp. 307–312, Mar./Apr. 2005.

[8] M. Peccianti, C. Conti, G. Assanto, A. De Luca, and C. Umeton, BAll optical switching and logic gating with spatial solitons in liquid crystals,[Appl. Phys. Lett., vol. 81, no. 18, pp. 3335–3337, Oct. 2002.

[9] A. Piccardi, A. Alberucci, G. Assanto, U. Bortolozzo, and S. Residori,BSoliton gating and switching in liquid crystal light valve,[Appl. Phys. Lett., vol. 96, no. 7, pp. 071104-1–071104-3, Feb. 2010.

[10] K. Mishina, A. Marta, S. Mitani, T. Miyahara, K. Ishida, K. Shimizu, T. Hatta, K. Motoshima, and K. Kitayama, "NRZ-OOK-to-RZ-BPSK modulation-format conversion using SOA-MZI wavelength converter,"J. Lightw. Technol., vol. 24, no. 10, pp. 3751–3758, Oct. 2006.

[11] Z. Liu, S. Xiao, L. Cai, and Z. Liang, "Multi-format receiver for nonreturn-to-zero binary-phase-shift-keyed and non-return-to-zero amplitude-shift-keyed signals," Opt. Exp., vol. 17, no. 4, pp. 2918–2925, Feb. 2009.

[12] M. L. Gilmore, F. R. Steel, and J. A. Tempka, "Digital Detection System for Differential Phase Shift Keyed Signal," U.S. Patent 3 993 956, Nov. 23, 1976

[13] C. Xu, X. Liu, and X. Wei, "Differential phase-shift keying for high spectral efficiency optical transmissions,"IEEE J. Sel. Top. Quantum Electron., vol. 10, no. 2, pp. 281–293, Mar./Apr. 2001.

[14] A. H. Gnauck and P. J. Winzer, "Optical phase-shift-keyed transmission,"J. Lightw. Technol., vol. 23, no. 1, pp. 115–130, Jan. 2005.

[15]P.A.Besse,M.Bachmann,H.Melchior,L.B.Soldano ,and M.K. Smit, "Optical bandwidth and fabrication tolerances of multimode interference couplers,"J. Lightw. Technol., vol. 12, no. 6, pp. 1001–1009, Jun. 1994

[16] J.Xiao,X.Liu,andX.Sum,"Design of an ultracompact MMI wavelength demultiplexer in slot waveguide structures,"Opt. Exp., vol. 15, no. 13, pp. 8300–8308, Jun. 2007.
[17] Y. Tsuji and M. Koshiba, "Finite element method using port truncation by perfectly matched layer boundary conditions for optical waveguide discontinuity problems,"J. Lightw. Technol., vol. 20, no. 3, pp. 463–468, Mar. 2002.
[18] O. A. Egorov, F. Lederer, and Y. S. Kivshar,BHow does an inclined holding beam affect discrete modulational instability and solitons in nonlinear cavities?[Opt. Exp., vol. 15, no. 7, pp. 4149–4158, Apr. 2007.
[19] B. Feng and T. Kawahara, Discrete Breathers in Two-Dimensional Nonlinear Lattices. Amsterdam, The Netherlands: Elsevier, 2007, ISSN: 0165-2125.
[20] L. B. Soldano and C. M. Pennings, "Optical multi-mode interference devices based on self-imaging: Principles and applications,"J. Lightw. Technol., vol. 13, no. 4, pp. 615–627, Apr. 1995.